

Supplementary Information

Low-Loss Aluminum Epitaxial Film for Scalable and Sustainable Plasmonics: Direct Comparison with Silver Epitaxial Film

Soniya S. Raja,^a Chang-Wei Cheng^b and Shangjr Gwo^{*abc}

^aInstitute of NanoEngineering and MicroSystems, National Tsing-Hua University, Hsinchu 30013, Taiwan

^bDepartment of Physics, National Tsing-Hua University, Hsinchu 30013, Taiwan

^cCenter for Applied Sciences, Academia Sinica, Nankang, Taipei 11529, Taiwan

*Corresponding author. E-mail: gwo@phys.nthu.edu.tw (S.G.)

Contents of Supplementary Information

Figure S1: Incident angle dependent white light interference patterns

Figure S2: Film thickness deepened SPP field distributions

Figure S3: White light interferometry curve fitting

Figure S4: White light interferometry measurement results on the silver epitaxial film

Figure S6: Direct laser scattering measurement results on the silver epitaxial film

Figure S5: Comparison with the literature results for the Al case

Figure S7: Schematics of optical measurement setups

Table S1: Drude-Lorentz model fitting parameters

Table S2: Optical dielectric function of aluminum and silver epifilms measured by two different methods

Table S3: Comparison between e-gun-grown and MBE-grown aluminum films

Table S4: Comparison of MBE-grown aluminum films by two methods

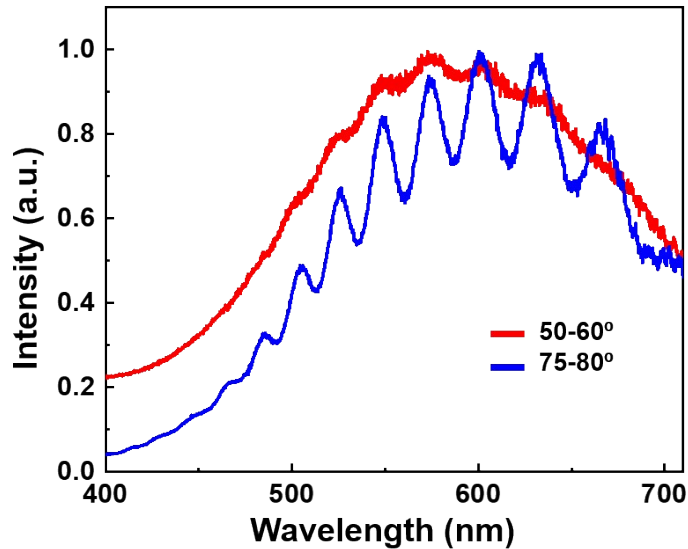


Figure S1. Interference patterns of the same pair of grooves (separated by a distance of $6 \mu\text{m}$) at different light source incident angles. We performed our measurements at the optimized angle of $75-80^\circ$, because at this angle the interference patterns are strong, compared to that at different angles shown in the figure. The strength and clarity of the peaks shows the importance of the optimized oblique angle of $75-80^\circ$. As the incident angle decreases the clarity of the interference pattern will also decrease.

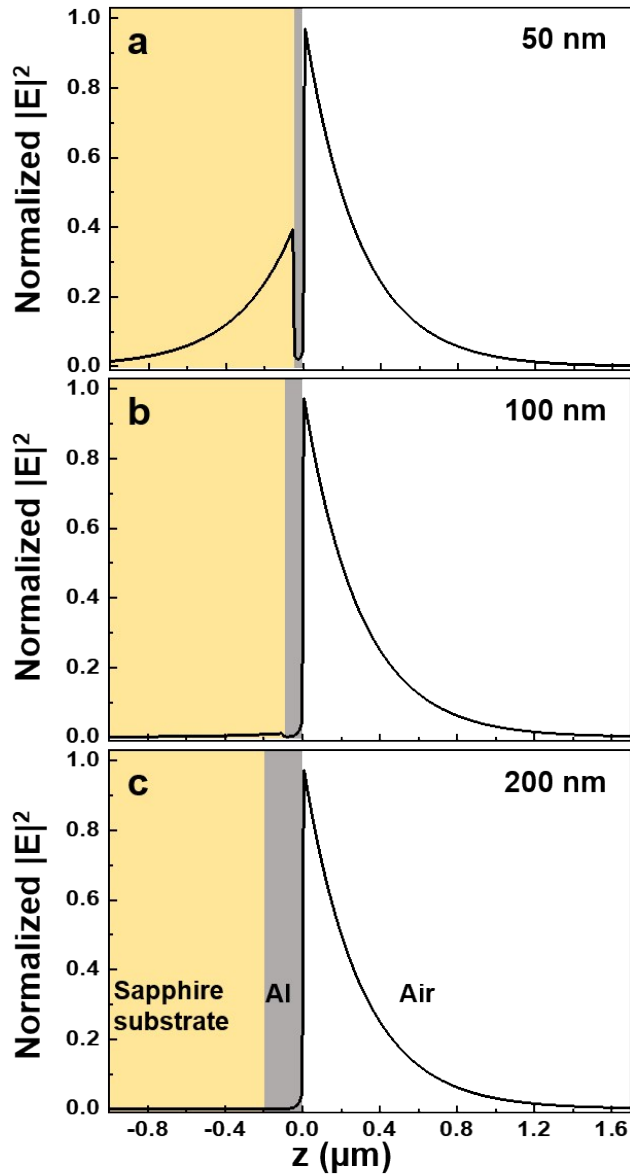


Figure S2. SPP field distributions with different thicknesses of aluminum films. We chose the film thickness of 200 nm to avoid a significant contribution from the leaky mode. The film thicknesses of (a) 50 nm (b) 100 nm (c) 200 nm are used for finite-difference time-domain (FDTD) simulations. We obtain the SPP modes by using the eigenmode solver software from Lumerical. The incident wavelength is $\lambda = 400 \text{ nm}$. The 50-nm-thick aluminum film exhibits a significant leaky mode, which can reduce the propagation length.

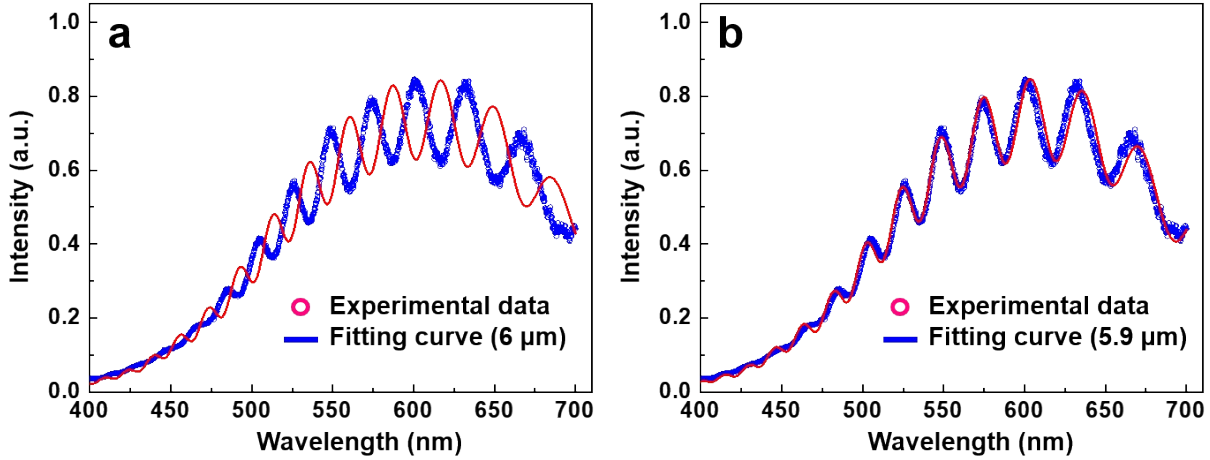


Figure S3. Example of WLI curve fitting for the determination of groove separation (D). (a) Curve fitting with $D = 6 \mu\text{m}$. (b) Curve fitting with $D = 5.9 \mu\text{m}$. The uncertainty of the D can be $\pm 100 \text{ nm}$. The separation was set during FIB fabrication of the grooves. After fabrication, the D value was confirmed by SEM image. However, the actual propagation distance between the grooves may vary by $\pm 100 \text{ nm}$. This is value to be determined during the curve fitting procedure as the example shown in this figure. Although the D value was measured as $6 \mu\text{m}$, the fitting curve does not match well with the experimental result. And the fitting curve seamlessly match when the D is $5.9 \mu\text{m}$. The other fitting parameters are the curve which covers the maxima of the interference fringe (I_{max}), the curve which covers the minima of the interference fringe (I_{min}) and the SPP reflectivity (r).

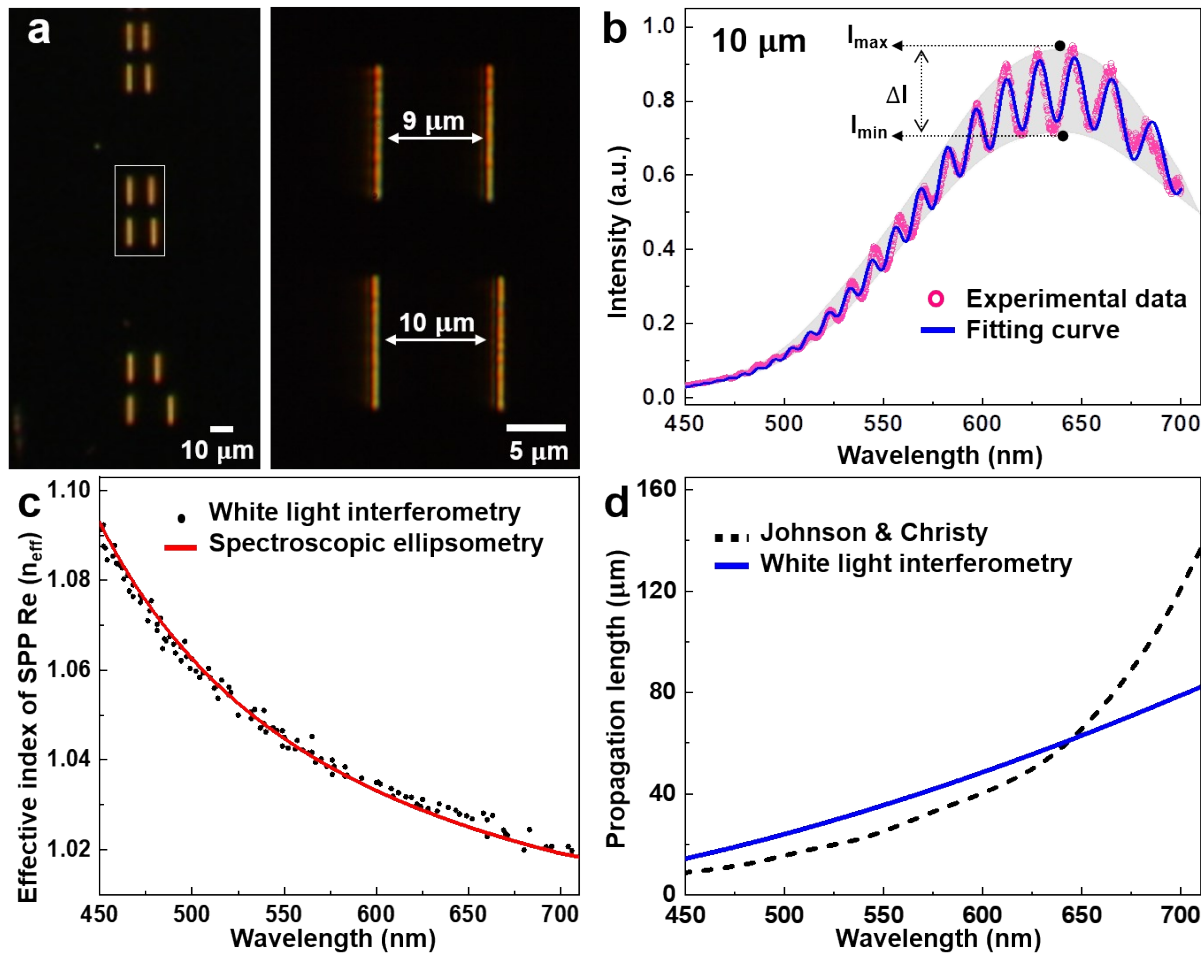


Figure S4. White light interferometry measurement on the silver epitaxial film. (a) Dark-field optical microscope image of the paired groove structures. (b) White light interference data recorded from two grooves of 10 μm separation. (c) Real part of the complex effective index of the epitaxial silver film extracted from the peaks and dips position of the white light interference data. (d) Propagation length on the silver epitaxial film surface obtained by the WLI method, compared with the propagation length derived from the Johnson and Christy (JC) data.^{S1} The apparent deviation in the long-wavelength region is due to the large uncertainties in the JC data.

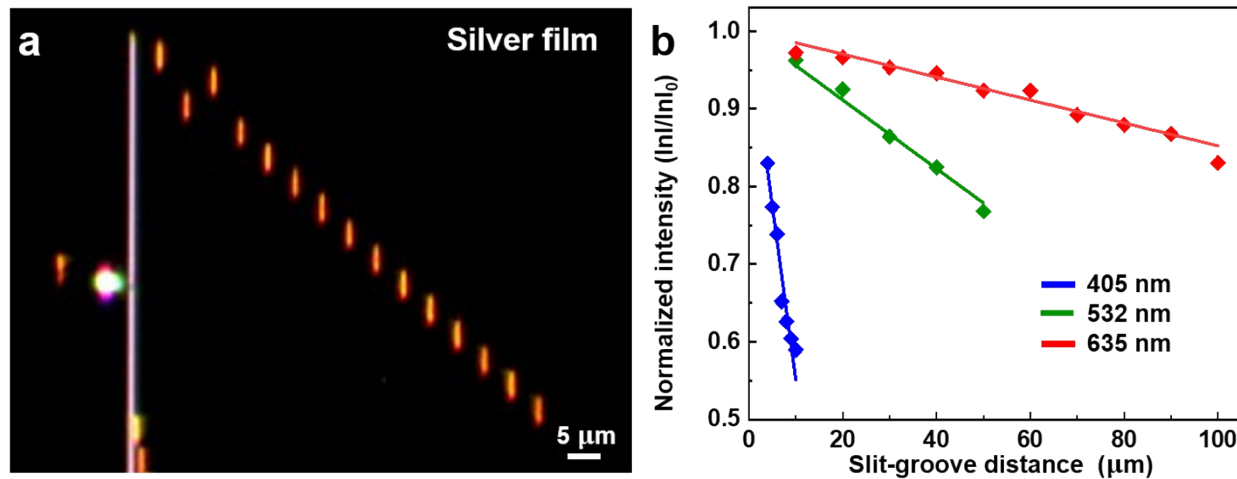


Figure S5. Direct laser scattering measurement on the silver epitaxial film. (a) Dark-field optical microscope image of slit-groove structures. (b) Scattered laser intensity from at the incident grooves as a function of distance from the distal grooves. The propagation lengths obtained by fitting the data points are 1 μm at 405 nm, 26 μm at 532 nm and 60 μm at 635 nm.

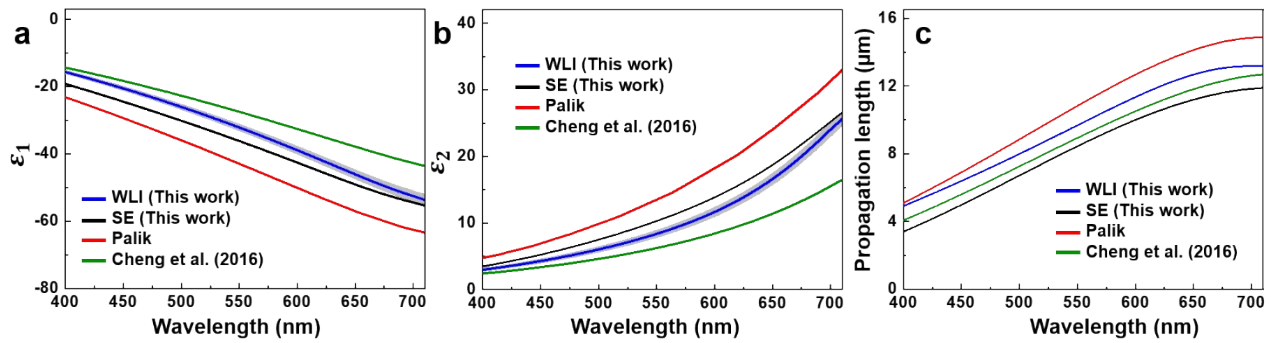


Figure S6. Comparison of experimentally measured dielectric function and propagation length of aluminum epitaxial film with previously published literature results. (a) Real (ϵ_1) and (b) imaginary (ϵ_2) parts of the dielectric function. (c) Propagation length of aluminum epitaxial film. These data were obtained from an aluminum epitaxial film by Cheng *et al.* (2016),⁸ Palik's Handbook of Optical Constants of Solids.^{S2}

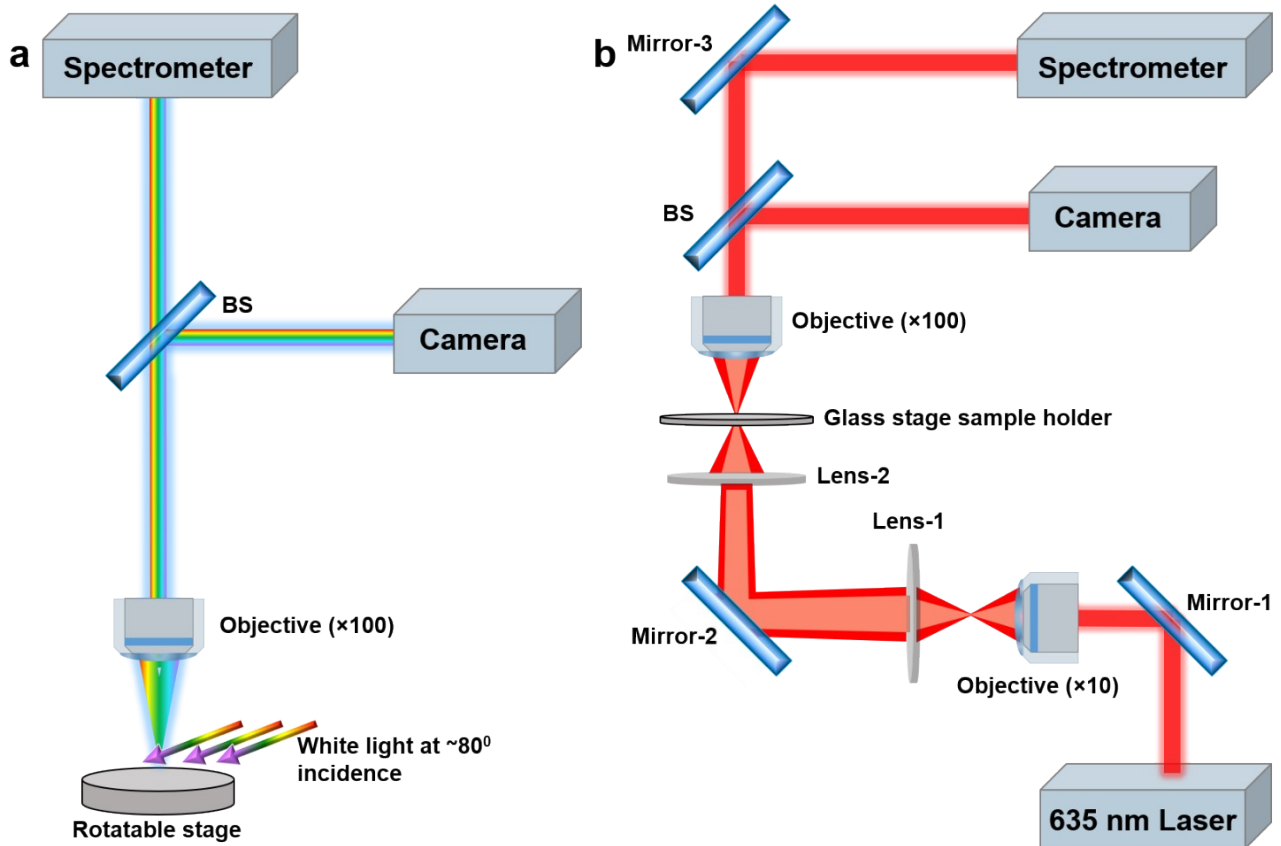


Figure S7. Schematics of the optical measurement setups used for (a) white light interferometry and (b) laser scattering methods.

Table S1. Drude-Lorentz fitting parameters used for the modeling.

$$\varepsilon(\omega) = \varepsilon_{bg} - \frac{\omega_p^2}{\omega(\omega + i\gamma_p)} + \sum_{j=1}^N \frac{A_j}{(\omega_j^2 - \omega^2 - i\omega\Gamma_j)},$$

where ε_b is the polarization response from the core electrons (background permittivity), ω_p is the bulk plasmon frequency, γ_p is the relaxation rate (electron-electron scattering loss), A_j is the strength, ω_j are the resonant frequencies of interband transitions and Γ_j are the damping rates of interband transitions (N is the number of interband transitions used for modeling).³⁵ These fitting parameters are valid only for the visible range of 400–700 nm.

	Aluminum		Silver	
	WLI	SE	WLI	SE
ε_{bg}	1	1	3.7	3.7
ω_p	12.32	12.32	9.0	9.2
γ_p	0.113	0.113	0.09	0.035
A_1	12.5	12.5	4.506	4.06
ω_1	1.548	1.548	4.2	4.2
Γ_1	0.33	0.33	0.22	0.22
A_2	45	28	20	
ω_2	2.2	1.88	5.585	
Γ_2	3.5	1.28	0.0066	
A_3	25		10	
ω_3	1.69		0.0004	
Γ_3	0.9		0.046	

Table S2. Optical Dielectric Function (Al and Ag) determined by two different methods (WLI and SE).

Wavelength (λ)	Epitaxial aluminum				Epitaxial silver			
	WLI		SE		WLI		SE	
	Real(ϵ)	Im(ϵ)						
400	-15.65	2.73	-19.20	3.49	-3.82	0.08	-4.44	0.17
405	-16.11	2.83	-19.70	3.64	-3.99	0.08	-4.70	0.18
410	-16.58	2.94	-20.21	3.79	-4.16	0.08	-4.95	0.18
415	-17.05	3.06	-20.73	3.96	-4.33	0.09	-5.21	0.19
420	-17.53	3.17	-21.25	4.12	-4.51	0.09	-5.47	0.19
425	-18.02	3.29	-21.78	4.29	-4.69	0.09	-5.73	0.20
430	-18.51	3.42	-22.31	4.47	-4.87	0.10	-5.99	0.20
435	-19.01	3.55	-22.84	4.65	-5.06	0.10	-6.25	0.21
440	-19.51	3.68	-23.38	4.84	-5.24	0.10	-6.52	0.21
445	-20.02	3.81	-23.92	5.03	-5.43	0.11	-6.78	0.22
450	-20.53	3.95	-24.47	5.23	-5.62	0.11	-7.05	0.22
455	-21.05	4.09	-25.02	5.43	-5.82	0.11	-7.32	0.23
460	-21.58	4.24	-25.58	5.64	-6.01	0.12	-7.59	0.24
465	-22.12	4.39	-26.13	5.85	-6.21	0.12	-7.86	0.24
470	-22.66	4.55	-26.70	6.07	-6.41	0.13	-8.13	0.25
475	-23.20	4.71	-27.26	6.30	-6.61	0.13	-8.41	0.25
480	-23.75	4.87	-27.83	6.52	-6.81	0.13	-8.69	0.26
485	-24.31	5.04	-28.40	6.76	-7.02	0.14	-8.97	0.27
490	-24.88	5.22	-28.98	7.00	-7.22	0.14	-9.26	0.27
495	-25.45	5.40	-29.56	7.24	-7.43	0.15	-9.54	0.28
500	-26.02	5.58	-30.14	7.49	-7.65	0.15	-9.83	0.28
505	-26.61	5.77	-30.73	7.74	-7.86	0.16	-10.12	0.29
510	-27.20	5.97	-31.32	8.00	-8.08	0.16	-10.41	0.30
515	-27.79	6.17	-31.91	8.27	-8.29	0.17	-10.71	0.30
520	-28.40	6.38	-32.51	8.54	-8.51	0.17	-11.01	0.31
525	-29.01	6.60	-33.11	8.82	-8.74	0.18	-11.31	0.32
530	-29.62	6.82	-33.72	9.10	-8.96	0.18	-11.61	0.32
535	-30.24	7.05	-34.33	9.39	-9.19	0.19	-11.91	0.33
540	-30.87	7.29	-34.94	9.68	-9.42	0.19	-12.22	0.34
545	-31.51	7.53	-35.56	9.98	-9.65	0.20	-12.53	0.34
550	-32.15	7.79	-36.18	10.29	-9.88	0.20	-12.85	0.35
555	-32.80	8.05	-36.80	10.61	-10.12	0.21	-13.16	0.36
560	-33.45	8.32	-37.43	10.93	-10.35	0.21	-13.48	0.37
565	-34.11	8.61	-38.06	11.26	-10.59	0.22	-13.80	0.37

570	-34.78	8.90	-38.70	11.60	-10.83	0.23	-14.12	0.38
575	-35.45	9.21	-39.34	11.95	-11.08	0.23	-14.45	0.39
580	-36.13	9.52	-39.99	12.31	-11.32	0.24	-14.78	0.40
585	-36.82	9.85	-40.64	12.67	-11.57	0.24	-15.11	0.40
590	-37.51	10.20	-41.29	13.05	-11.82	0.25	-15.44	0.41
595	-38.20	10.55	-41.94	13.45	-12.07	0.26	-15.78	0.42
600	-38.91	10.93	-42.60	13.85	-12.33	0.26	-16.12	0.43
605	-39.61	11.31	-43.26	14.27	-12.59	0.27	-16.46	0.43
610	-40.32	11.72	-43.92	14.70	-12.84	0.28	-16.80	0.44
615	-41.04	12.14	-44.58	15.14	-13.10	0.28	-17.15	0.45
620	-41.76	12.58	-45.24	15.60	-13.37	0.29	-17.50	0.46
625	-42.48	13.05	-45.89	16.08	-13.63	0.30	-17.85	0.47
630	-43.20	13.53	-46.55	16.58	-13.90	0.30	-18.21	0.47
635	-43.93	14.04	-47.20	17.09	-14.17	0.31	-18.57	0.48
640	-44.65	14.57	-47.84	17.62	-14.44	0.32	-18.93	0.49
645	-45.37	15.13	-48.48	18.16	-14.71	0.33	-19.29	0.50
650	-46.09	15.71	-49.10	18.73	-14.99	0.33	-19.65	0.51
655	-46.80	16.31	-49.72	19.31	-15.27	0.34	-20.02	0.52
660	-47.50	16.95	-50.32	19.91	-15.55	0.35	-20.39	0.53
665	-48.20	17.61	-50.90	20.53	-15.83	0.36	-20.77	0.54
670	-48.88	18.30	-51.47	21.16	-16.11	0.37	-21.15	0.54
675	-49.54	19.02	-52.02	21.81	-16.40	0.37	-21.53	0.55
680	-50.19	19.76	-52.55	22.47	-16.69	0.38	-21.91	0.56
685	-50.82	20.53	-53.06	23.15	-16.98	0.39	-22.29	0.57
690	-51.42	21.32	-53.55	23.83	-17.27	0.40	-22.68	0.58
695	-51.99	22.13	-54.01	24.52	-17.56	0.41	-23.07	0.59
700	-52.54	22.95	-54.45	25.22	-17.86	0.42	-23.46	0.60

Table S3. Comparison of surface roughness, optical reflectivity and loss (ϵ_2 , the imaginary part of dielectric function) of MBE-grown, single-crystalline Al film and electron-gun (e-gun) evaporated polycrystalline Al film at wavelength 400 nm.

	E-gun evaporated^{S3}	MBE-grown^{S3}	MBE-grown (this work)
Crystalline nature	Poly-crystalline	Single-crystalline	Single-crystalline
Surface roughness (RMS)	2.5 nm	0.65 nm	0.5 nm
Reflectivity @ $\lambda = 400$ nm	0.78	0.89	0.9
Loss (ϵ_2) @ $\lambda = 400$ nm	8	5	3

Table S4. Comparison between two growth mechanisms of MBE-grown Al films.

	MBE-grown (this work)	MBE-grown (Cheng <i>et al.</i>)⁸
Growth method	Single-step growth at RT	Two-step growth
Growth temperature	Room temperature	Low temperature (90 K) + Room temperature (anneal)
Crystalline nature	Single-crystalline	Single-crystalline
Surface roughness	0.5 nm	0.26 nm
Growth rate	33.3 Å/min	4.7 Å/min
Growth environment	$\sim 1 \times 10^{-10}$ Torr	Below 1×10^{-10} Torr

Additional References:

- S1. P. B. Johnson and R. W. Christy, Optical Constants of the Noble Metals. *Phys. Rev. B*, 1972, **6**, 4370–4379.
- S2. E. D. Palik, *Handbook of Optical Constants of Solids*; Academic press handbook, San Diego, 1985, **1**, 404-406.
- S3 Y. C. Chung, P. J. Cheng, Y. H. Chou, B. T. Chou, K. B. Hong, J. H. Shih, S. D. Lin, T. C. Lu, T. R. Lin, *Sci. Rep.*, 2017, **7**, 39813.